DFT study on the gold(I)-catalyzed cycloaddition and rearrangement reactions of allene-containing allylic silyl ether

Yamei Zhao (zhaoyamei135@126.com)
Xi'an Polytechnic University
MengDan Huo
Xi'an Polytechnic University
HongJi Zhou
Xi'an Polytechnic University

Research Article

Keywords: gold(I)-catalyzed, cycloaddition, rearrangement, spirocyclo[4,5]decane

Posted Date: March 29th, 2021

DOI: https://doi.org/10.21203/rs.3.rs-264195/v1

Version of Record: A version of this preprint was published at Journal of Molecular Modeling on December 31st, 2021. See the published version at https://doi.org/10.1007/s00894-021-05004-8.

Abstract

The DFT calculation of the B3LYP level was carried out to explore the reaction mechanism of the synthesis of spirocyclo[4, 5]decane skeleton by gold-catalyzed allenyl compounds. The more accurate energy under the CH3CN solvent in the experiment is calculated by the single point energy of the SMD model. Computational studies have shown that the reaction consists of three main steps: intramolecular cycloaddition of the end group carbon atoms of allenyl and vinyl groups, the semipinacol rearrangement process in which the four-membered ring is reconstructed into the five-membered ring, the elimination reaction releases the catalyst and obtains the product. The calculation results show that Zheng et al. reported that the gold-catalyzed synthesis reaction can easily occur under the experimental conditions due to its low activation free energy (12.42–16.79 kcal/mol). Furthermore, it was found that the MOMO$(CH_2)_2$ substituent has higher reactivity than the corresponding reactant of the phenyl substituent.

1. Introduction

Molecules with a spirocyclo[4, 5]decane skeleton have good biological properties due to the important moiety of the quaternary carbon center, which is widely present in various pharmaceutical molecules and natural bioactive products, such as spirojatamol, erythrodiene and cedrene, etc [1–6]. However, the key part of the structure of the scaffold containing quaternary carbon is difficult to construct directly in the synthesis due to the large steric repulsion [7–11]. The development of an effective synthesis method is also one of the synthesis problems that need to be overcome, and it has also attracted a large number of chemists to carry out related research work [12–15]. Over the years, some synthetic methods have been developed and molecular functionalization studies have been carried out. Especially intramolecular cycloaddition or intermolecular cycloaddition reaction is mostly, such as intramolecular dearomatization cyclization of phenols [16], photo-induced intramolecular [2 + 2] cyclization [17], intermolecular [4 + 2] or [3 + 2] cycloaddition [18–19]. In addition, in order to further improve the reaction efficiency and enhance the diversity of product structures, transition metal catalysis and rearrangement reactions are also widely used in the synthesis of such products. The semipinacol rearrangement is also considered to be a very effective method to build a quaternary carbon skeleton through migration or recombination. Studies have reported that both vinylogous *α*-ketol and *α*-hydroxy epoxide alcohol have been used to construct spirocyclo [4.5] decane skeletons through semipinacol rearrangement [20–22].

In order to further explore new rearrangement modes for introducing the required functional groups more effectively, recent studies by Zheng *et al*. found that Au(I)-catalyzed allyl alcohol compounds (**a** or **b**) can easily undergo intramolecular cyclization / semipinacol rearrangement reaction, and high yields (95% and 65%) of spirocyclic [4.5]-decane skeleton (Scheme 1) can be generated by Au(PPh_3)Cl catalyst in CH_3CN solution at room temperature [23]. Based on the experimental research results of Zheng's research team, a key intermediate was given to predict the possible reaction process. In order to further explore the detailed catalytic reaction mechanism, a feasible channel was given to synthesize spirocyclo[4.5]decane skeleton of quaternary carbon center from allene-containing allylic silyl ether (Scheme 2). First, the allylic alcohols reactant (**a)** is activated by Au(I) $^+$ catalyst to obtain intermediate **I**. Then, the allene group and

the terminal carbon of the vinyl group undergo intramolecular cyclization to form intermediate **II**. Next, a rearrangement reaction occurred on the four-membered ring in intermediate **II** and the corresponding five-membered ring intermediate **III** was formed, which is also the possible intermediate structure mentioned in the experimental report. Finally, water molecules are added to the intermediate **III** to obtain the final product **a-p** and release the gold (I) catalyst and TESOH molecules.

As far as we know, there is no relevant theoretical research report to explain the new gold-catalyzed synthesis of quaternary carbon-containing framework from allenes reported by Zheng and co-workers. In this article, based on the experimental phenomenon of *Zheng et al*., we carried out a calculation study of the density functional theory B3LYP method on the mechanism of the cyclization and rearrangement of allene-containing allylic silyl ether catalyzed by gold (I) catalyst. We hope to clarify the specific reaction mechanism and learn more about the factors that control the activity of this reaction through theoretical research.

2. Computational Details

The DFT calculations [24] of all research systems are performed using Gaussian 09 software [25]. Both geometric optimization and frequency calculation are done using the B3LYP calculation method [26] of density functional theory. The SDD basis set containing the effective core relativistic pseudo potential [27] is selected for the Au, while other atoms applied 6-31G (*d, p*) basis set [28]. We also determined and verified the TS structure to correctly connect the two corresponding stable structures through IRC calculations [29]. In order to obtain the precise energy corresponding to the experimental reaction solvent system, we used a larger basis set to recalculate the single-point energy of all optimized geometries in the corresponding experimental solvents. This is also a widely used method to obtain accurate energy in catalytic reactions [30–34]. The larger basis set of 6-311 + + G (*d, p*) (SDD with ECP for Au) in the SMD implicit solvent environment [35] with acetonitrile (solvent = CH_3CN, $\varepsilon = 35.688$) is used. All energy values discussed in the context are relative Gibbs energy (kcal/mol) corrected by the single-point energy of solvation. The three-dimensional (3D) structures were obtained directly from the calculated output using CYLview software.

3. Results And Discussion

For this catalytic synthesis reaction, experimental studies have proved that $Au(PPh_3)Cl$ is the most effective gold catalyst. According to the experimental conditions, theoretical calculations are based on $Au(PPh_3)^+$ as the catalyst model, which interacts with the allene reactant **a** in Scheme 1 and the terminal unsaturated bond is activated to obtain the initial reaction complex **1a-int**. The frontier molecular orbital and the electrostatic potential diagram of the reaction complex **1a-int** are shown in Fig. 1. It can be seen from the LUMO molecular orbital that the π electrons on the terminal C = C double bond of the allene group in the molecule **1a-int** are filled on the *d* orbital of Au^+, the π bond is activated and the electrons on the orbital have a large overlap degree. In addition, on the two molecular orbitals of HOMO and HOMO-1,

the non-terminal carbon-carbon double bond in the allene group and the vinyl group in the molecule have strong π electrons, especially the vinyl group is easy to interact with activated carbon-carbon bond of the allene group undergoes an intramolecular cycloaddition reaction to complete the ring closure. The energy gap between the HOMO and LUMO orbitals of the molecule is 0.16 hartree, and the smaller energy difference helps the electron transition to complete the cyclization process. The electrostatic potential diagram clearly shows that most of the atoms in the molecule are electropositive, only three oxygen atoms and the π system show weak electronegativity. In the calculation study of this reaction process, **1a-int** was used as the initial reaction complex to explore the specific reaction mechanism.

3.1 Reaction Mechanism

The free energy profiles of gold(I)-catalyzed intramolecular cycloaddition and rearrangement reactions starting from reactant **1a-int** is given in Fig. 2. The key geometric geometries giving the main structural parameters are shown in Fig. 3. In **1a-int**, the two new gold-carbon bonds Au-C1 and Au-C2 formed by the gold(I) ion and allene group are 2.403 and 2.276 Å respectively. The C1-C2 bond is also further activated by $Au(PPh_3)^+$, elongating to 1.360 Å. From Fig. 2 along the initial complex 1a-int, the allene group and the terminal carbon atom of the vinyl group undergo an intramolecular cycloaddition reaction through the transition state **12a-ts** to form the intermediate **2a-int**. At the same time, the gold atom also transferred to the middle carbon atom of the allene group. The only imaginary frequency of **12a-ts** is 255.04 i cm^{-1} and the energy barrier of this step is 12.42 kcal/mol relative to **1a-int**, and the energy of **2a-int** is 2.42 kcal/mol. In **12a-ts**, the distance of the interacting C1-C3 bond is 2.075 Å, the Au atom is also completely transferred to the C2 atom and the Au-C2 bond is shortened to 2.128 Å, while the C1-C2 bond is stretched to 1.449 Å. From **1a-int** to **2a-int**, the unsaturated group completes the ring closure to form a cyclohexene six-membered ring structure 2a**-int**, and the C1 and C3 atoms are also transformed from sp^2 to sp^3 hybridization. The C1-C2 and C1-C3 bonds both exhibit the characteristics of a single bond, and the bond lengths in **2a-int** are 1.517 and 1.563 Å respectively. However, the four-membered ring skeleton in the **2a-int** structure still has certain instability. He can easily construct the four-membered ring into a more stable five-membered ring through the semipinacol rearrangement process of the transition state **23a-ts** (imaginary frequency is 194.93 i cm^{-1}) to obtain a more stable intermediate **3a-int**. The activation free energy of this step is 9.59 kcal/mol relative to the intermediate **2a-int**. For **23a-ts**, the C5-C6 bond tends to dissociate and stretch to 1.758 Å, and C4-C6 has a tendency to form bonds, with a bond length of 2.239 Å. The formation of **3a-int** structure indicates that the rearrangement process has been completed, and its energy is reduced by 26.23kcal/mol compared to **2a-int**, which is a step of strong exothermic process. The spirocyclo[4.5]decane skeleton has been initially formed in the **3a-int** structure. The C4 atom transitions to the sp^3 hybrid mode and the newly formed C4-C6 bond is 1.554 Å. The six-membered ring and the five-membered ring form two planes that are approximately perpendicular to each other. Then, the H^+ in the water in the reaction system attacks the intermediate **3a-int** through the transition state **34a-ts** to obtain the intermediate **4a-int** and release the catalyst $Au(PPh_3)^+$. The activation energy of this step is relatively low with 4.44 kcal/mol, The energy of the step of generating **4a-int** is almost unchanged and only reduced by 1.62 kcal/mol. The only virtual frequency in **34a-ts** is 768.64 i cm^{-1}, and its vibration

mode is mainly shown in the H between Au and C2 atoms, where the Au-H and H-C2 bond lengths are 1.834 and 1.826 Å, respectively. Finally, the excess OH^- in the water interacts with the intermediate **4a-int** to remove the TESOH molecule to obtain the final product **a-p**, whose energy continues to decrease by 3.44kcal/mol.

Throughout the entire catalytic reaction process, the first step of the intramolecular cycloaddition process is the rate-determining step of the entire reaction, and its energy is relatively low at 12.42 kcal/mol. This is consistent with the experimental results that the synthesis reaction can be carried out under the reaction conditions at room temperature, and the product with a high yield of 95% can be obtained. The activation free energy of the second key step of semipinacol rearrangement is lower than that of the first step, and the reaction process of the second step is easier to complete. Moreover, the entire reaction is also an exothermic process with an exothermic amount of 28.87 kcal/mol. This provides a good explanation for the detailed reaction mechanism reported by Zheng et al.

3.2 The influence of the substituents on the reactant allenyl group

According to experimental reports, in order to further investigate the influence of substituents on the reactivity, the $MOMO(CH_2)_2$ group in the reaction substrate **a** was replaced by a phenyl group as a new reactant **b** (Scheme 1), and the reaction mechanism was studied by the same theoretical calculation method. The specific reaction process and mechanism similar to the reaction substrate **a** is shown in Fig. 4. The geometric structure containing the main parameters is shown in Fig. 5. In the reaction complex **1b-int**, the newly formed Au-C1 bond is 0.018 Å longer than that of **1a-int**, while the Au-C2 bond is shorter than the corresponding one by 0.025 Å. It can be clearly seen from Fig. 4 that starting from the complex **1b-int** and going through the transition states **12b-ts**, **23b-ts** and **34b-ts** along the reaction path, it also goes through three steps, namely intramolecular cycloaddition, semipinacol rearrangement and the elimination process of releasing the catalyst, etc. The activation free energy of the three steps is 16.79, 12.49 and 5.13kcal/mol respectively, which are 4.37, 2.90 and 0.69kcal/mol higher than the activation free energy of the **1a-int** reaction channel respectively. The reaction system shows that the cycloaddition process (the first step) is still the rate-determining step of the entire catalytic reaction process, and its reaction barrier is also slightly higher than **1a-int**. This reaction channel is also a strong exothermic process, and its exothermic heat is almost the same as that of the **1a-int** reaction channel, its value is -29.59 kcal/mol, which is only 0.72kcal/mol higher. From the structural point of view, the basic skeleton of the intermediate and transition state structure is basically similar to that of the **1a-int** reaction channel, except that the phenyl group replaces the $MOMO(CH_2)_2$- group to cause systematic changes in some parameters. The IRC calculation results confirm that **12b-ts**, **23b-ts**, and **34b-ts** are connected to the corresponding intermediates **1b-int**, **2b-int**, **3b-int** and **4b-int**, respectively.

The Au(I)-catalyzed reaction of allene-containing allylic silyl ether to synthesize spirocyclo[4.5]decane skeleton has lower activation free energy (channels a and b are 12.42 and 16.79 kcal/mol, respectively). Moreover, the reaction barrier of intramolecular cycloaddition is higher than that of semipinacol rearrangement. However, comparing the reactivity of gold-catalyzed substrates with two different substituents, it is obvious that the activation barrier of $MOMO(CH_2)_2$- is 4.37 kcal/mol lower than that of

phenyl, and it has higher reactivity. The calculated results can well support the experimental report results. The experiment shows that the yields of the two products **a-p** and **b-p** are 95% and 65%, respectively. This experimental phenomenon is also consistent with the calculation result that the product **a-p** has a lower activation energy, and the product **b-p** has a higher energy barrier.

4. Conclusion

In this work, we provide detailed calculation studies and theoretical analysis of DFT (B3LYP) level for the synthesis of spirocyclo[4.5]decane skeleton catalyzed by gold complexes. Detailed calculations and precise parameters of the geometry and energy of the intermediates and transition states on the reaction channel are given. Based on the experimental report of Zheng et al., the optimal reaction path of the catalytic reaction was given, including three main steps: intramolecular cycloaddition, semipinacol rearrangement, and elimination of the release catalyst. The first step of the reaction, the cycloaddition process is the rate determining step of the entire catalytic cycle. Studies have found that this type of reaction has relatively low activation free energy, and the reaction barrier for the product a-p is 12.42 kcal/mol. For gold catalyst substrates with two different substituents, MOMO(CH2)2- is more reactive than phenyl. The detailed theoretical calculation results are completely consistent with the experimental phenomenon, which provides a good explanation and supplement for the experimental research.

Declarations

Acknowledgments We are grateful to the reviewers for their invaluable suggestions.

Funding This work was supported the Special Research PLan of Shaanxi Provincal Department of Education, China (No.18JK0340).

Conflict of interest

The authors declare that they have no competing interests.

Ethics approval

Consent to participate

Consent for publication

Written informed consent for publication was obtained from all participants.

Availability of data and material:

Not applicable.

Code availability

Contributions:

YaMei Zhao: Problem selection, writing and data analysis.

MengDan Huo : Methods, project management, result analysis, manuscript editing.

HongJi Zhou: Data analysis, writing.

References

1. Saraswat P, Jeyabalan G, Hassan MZ, Rahman MU, Nyola NK(2016) Review of synthesis and various biological activities of spiro heterocyclic compounds comprising oxindole and pyrrolidine moities. Synth Commun 46:1643–1664
2. Zheng Y, Tice CM, Singh SB (2014) The use of spirocyclic scaffolds in drug discovery. Bioorg Med Chem Lett 24:3673–3682
3. Ding K, Han Z, Wang Z (2009) Spiro skeletons: a class of privileged structure for chiral ligand design. Chem- Asian J 4: 32–41
4. Tokunaga Y, Yagihashi M, Ihara M, Fukumoto K (1995) A simple total synthesis of (±)-spirojatamol and (±)-erythrodiene via intramolecular 1,3-dipolar cycloaddition. J Chem Soc, Chem Commun 0: 955–956
5. Pathirana C, Fenical W, Corcoran E, Clardy J (1993) Erythrodiene: a new spirobicyclic sesquiterpene of a rare skeletal class from the caribbean gorgonian coral erythropodium caribaeorum. Tetrahedron Lett 34:3371–3372
6. Bagchi A, Oshima Y, Hikino H (1990) Spirojatamol, a new skeletal sesquiterpenoid of nardostachys jatamansi roots. Tetrahedron 46: 1523–1530
7. Zhuo S, Zhu T, Zhou L, Mou C, Chai H, Lu Y, Pan L, Jin Z, Chi YR (2019) Access to all-carbon spirocycles through a carbene and thiourea cocatalytic desymmetrization cascade reaction. Angew Chem Int Ed 58:1784–1788
8. Li Y, Xu S (2018) Transition-metal-catalyzed C-H functionalization for construction of quaternary carbon centers. Chem- Eur J 24: 16218–16245
9. Li S, Zhang JW, Li X L, Cheng DJ, Tan B (2016) Phosphoric acid-catalyzed asymmetric synthesis of spinol derivatives. J Am Chem Soc 138: 16561–16566
10. Rahemtulla BF, Clark HF, Smith MD (2016) Catalytic enantioselective synthesis of C1 - and C2 - symmetric spirobiindanones through counterion-directed enolate C-acylation. Angew Chem Int Ed 55: 13180–13183
11. Quasdorf KW, Overman LE (2014) Catalytic enantioselective synthesis of quaternary carbon stereo-centres. Nature 516: 181–191
12. Xu PW, Yu JS, Chen C, Cao ZY, Zhou F, Zhou J (2019) Catalytic enantioselective construction of spiro quaternary carbon stereocenters. ACS Catal 9: 1820–1882

13. Ding A, Meazza M, Guo H, Yang JW, Rios R (2018) New development in the enantioselective synthesis of spiro compounds. Chem Soc Rev 47: 5946–5996
14. Smith LK, Baxendale IR (2015) Total syntheses of natural products containing spirocarbocycles. Org Biomol Chem 13: 9907–9933
15. D'Yakonov VA, Trapeznikova OA, de Meijere A, Dzhemilev UM (2014) Metal complex catalysis in the synthesis of spirocarbocycles. Chem Rev 114: 5775–5814
16. Nemoto T, Ishige Y, Yoshida M, Kohno Y, Kanematsu M, Hamada Y (2010) Novel method for synthesizing spiro [4.5] cyclohexadienones through a Pd-catalyzed intramolecular ipso-friedel-crafts allylic alkylation of phenols. Org Lett 12: 5020–5023
17. Poplata S, Bauer A, Storch G, Bach T (2019) Intramolecular [2 +2] photocycloaddition of cyclic enones: selectivity control by lewis acids and mechanistic implications. Chem-Eur J 25: 8135–8148
18. Donslund BS, Nielsen RP, Monsted SM, Jorgensen KA (2016) Benzofulvenes in trienamine catalysis: stereoselective spiroindene synthesis. Angew Chem Int Ed 55: 11124–11128
19. Zhang G, Zhang L(2008) Au-containing all-carbon 1,3-dipoles:generation and [3 + 2] cycloaddition reactions. J Am Chem Soc 130: 12598–12599
20. Zhang XM, Tu YQ, Zhang FM, Chen Z H, Wang SH (2017) Recent applications of the 1,2-carbon atom migration strategy in complex natural product totalSynthesis. Chem Soc Rev 46: 2272–2305
21. Wang SH, Li BS, Tu YQ (2014) Catalytic asymmetric semipinacol rearrangements. Chem Commun 50: 2393–2408
22. Song ZL, Fan CA,Tu YQ (2011) Semipinacol rearrangement in natural product synthesis. Chem Rev 111: 7523–7556
23. Zheng TL, Zhang Y, Gou AL, Cheng F, Liu SZ, Yu L, Cui MY, Xu XT, Zhang K, Wang SH (2020) Au(I)-catalyzed cyclization/semipinacol rearrangement reaction of allenes to construct quaternary carbon-containing scaffolds. Org Lett 22: 7073–7077
24. Parr RG, Yang W (1989) Density-functional theory of atoms and molecules. Oxford University Press, New York.
25. Frisch MJ, Trucks GW, Schlegel HB, Scuseria GE, Robb MA, Cheeseman JR, Scalmani G, Barone V, Mennucci B, Petersson GA, Nakatsuji H, Caricato M, Li X, Hratchian HP, Izmaylov AF, Bloino J, Zheng G, Sonnenberg JL, Hada M, Ehara M, Toyota K, Fukuda R, Hasegawa J, Ishida M, Nakajima T, Honda Y, Kitao O, Nakai H, Vreven T, Montgomery JA, Peralta JE, Ogliaro F, Bearpark M, Heyd JJ, Brothers E, Kudin KN, Staroverov VN, Kobayashi R, Normand J, Raghavachari K, Rendell A, Burant JC, Iyengar SS, Tomasi J, Cossi M, Rega N, Millam JM, Klene M, Knox JE, Cross JB, Bakken V, Adamo C, Jaramillo J, Gomperts R, Stratmann RE, Yazyev O, Austin AJ, Cammi R, Pomelli C, Ochterski JW, Martin RL, Morokuma K, Zakrzewski VG, Voth GA, Salvador P, Dannenberg JJ, Dapprich S, Daniels AD, Farkas O, Foresman JB, Ortiz JV, Cioslowski J, Fox DJ (2009) Gaussian 09, Revision A.01; Gaussian, Inc., Wallingford CT.
26. Stephens PJ, Devlin FJ, Chabalowski CF (1994) Ab initio calculation of vibrational absorption and circular dichroism spectra using density functional force fields. J Phys Chem 98:11623–11627

27. Andrae D, Haussermann U, Dolg M, Stoll H, Preuss H (1990) Energy-adjusted ab initio pseudopotentials for the second and third row transition elements. Theor Chim Acta 77:123–141
28. Rassolov VA, Ratner MA, Pople JA, Redfern PC, Curtiss LA (2001) 6-31G* basis set for third-row atoms. J Comput Chem 22: 976–984.
29. Gonzalez C, Schlegel HB (1989) An improved algorithm for reaction path following. J Chem Phys 90: 2154–2161.
30. Zhang XH, Li SS, Wei XL, Lei Y (2018) Computational study of Ru-catalyzed cycloisomerization of 2-alkynylanilides. J Mol Model 24:162
31. Zhang XH,Wu, X, Lei Y (2019) Theoretical study on reaction mechanism of synthesis of iridium complexes having cyclometalated acyclic diaminocarbene ancillary ligands. J Mol Model 25: 262
32. Dar SA (2020) Investigation of electronic, magnetic, elastic, mechanical, thermodynamic, and thermoelectronic properties of Mn_2PtV Heusler alloy: ab initio study. J Mol Model 26: 35
33. Wild S, Tice N (2021) DFT study of structural and electronic properties of 1,4-diarylcyclopenta[d] pyridazines and oxazines for non-linear optical applications. J Mol Model 27: 60
34. Abedini N, Kassaee MZ (2020) A theoretical investigation into novel germylenes: effects of nitrogen substitution on stability and multiplicity. J Mol Model 26:325
35. Marenich AV, Cramer CJ, Truhlar DG (2009) Universal salvation model based on solute electron density and on a continuum model of the solvent defined by the bulk dielectric constant and atomic surface tensions. J Phys Chem B 113:6378–6396
36. Legault, C. Y. CYLview, 1.0b. Université de Sherbrooke: Sherbrooke, Quebec, Canada, 2009. www.cylview.org.

Figures

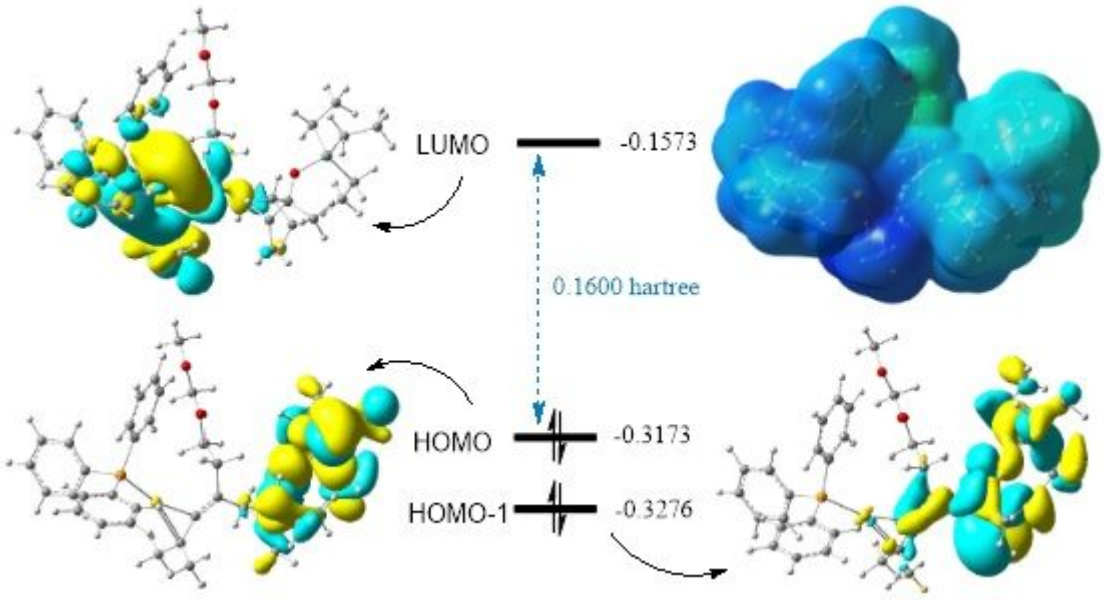

Figure 1

Frontier molecular orbital and electrostatic potential diagram of the complex 1a-int

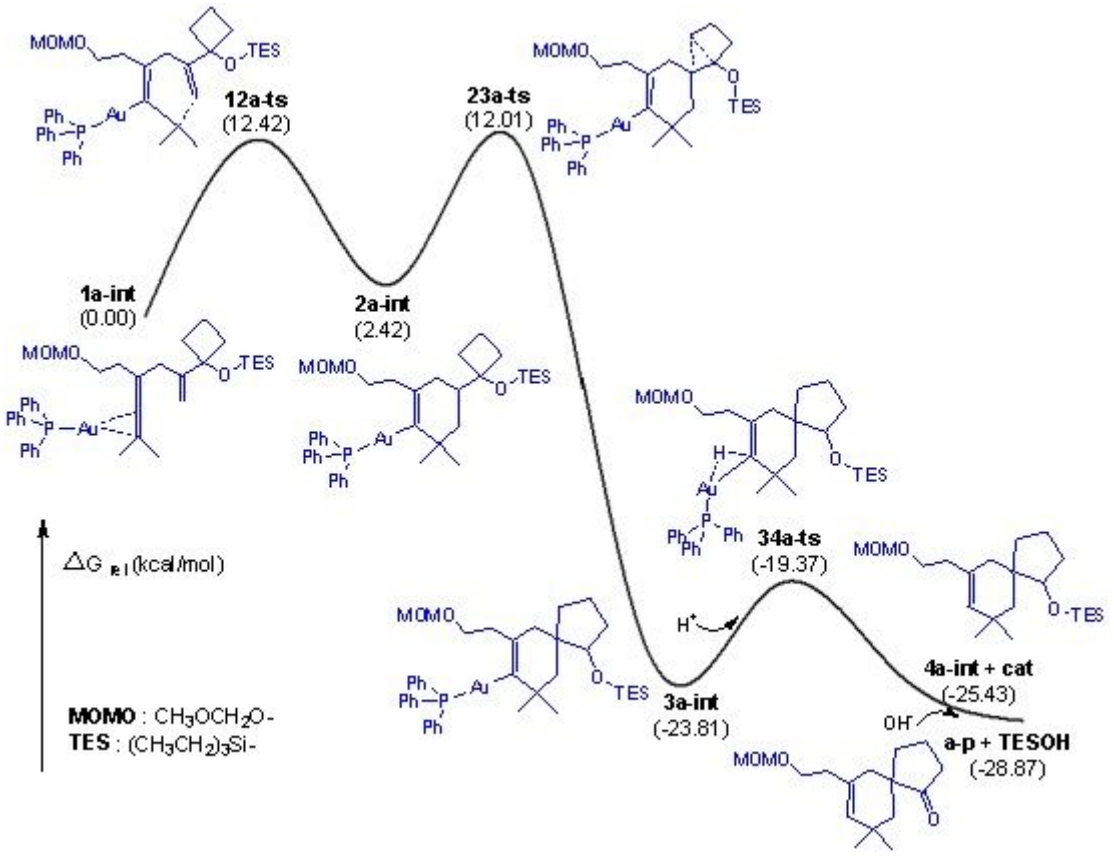

Figure 2

Gibbs free energy profiles for the Au(I)-catalyzed intramolecular cyclization and rearrangement of reactant a (R = MOMOCH2CH2- in Scheme 1). The energies are given in kcal/mol.

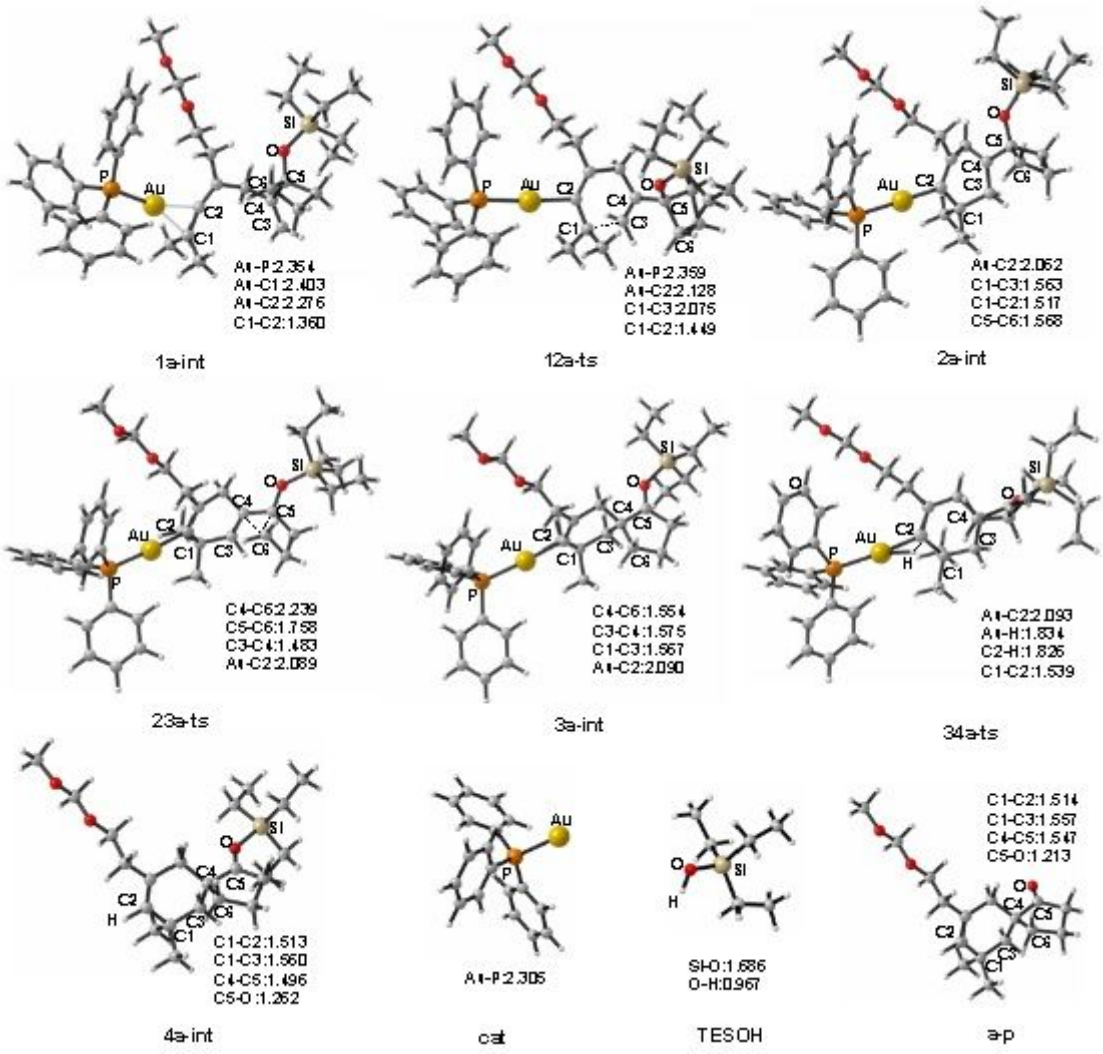

Figure 3

The optimized structures with the key bond lengths in Å for pathway a are shown in Fig. 2.

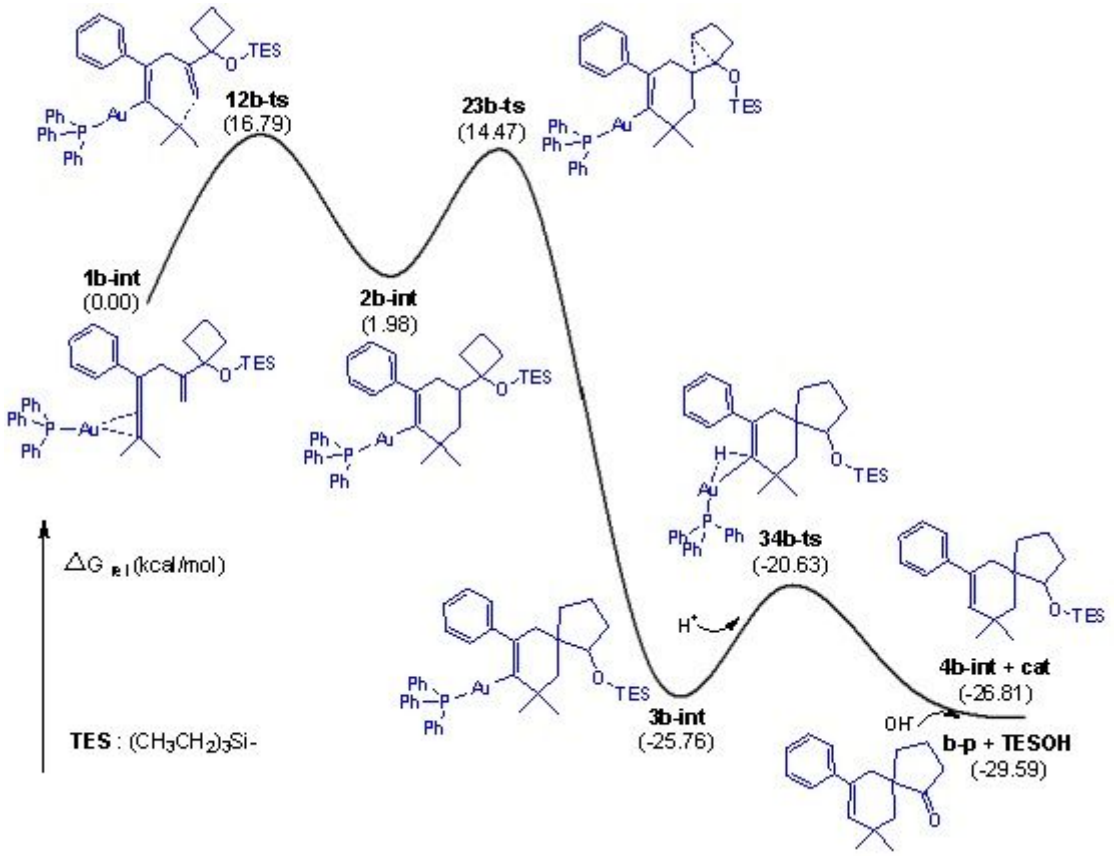

Figure 4

Gibbs free energy profiles for the Au(I)-catalyzed intramolecular cyclization and rearrangement of reactant a (R = Ph in Scheme 1). The energies are given in kcal/mol

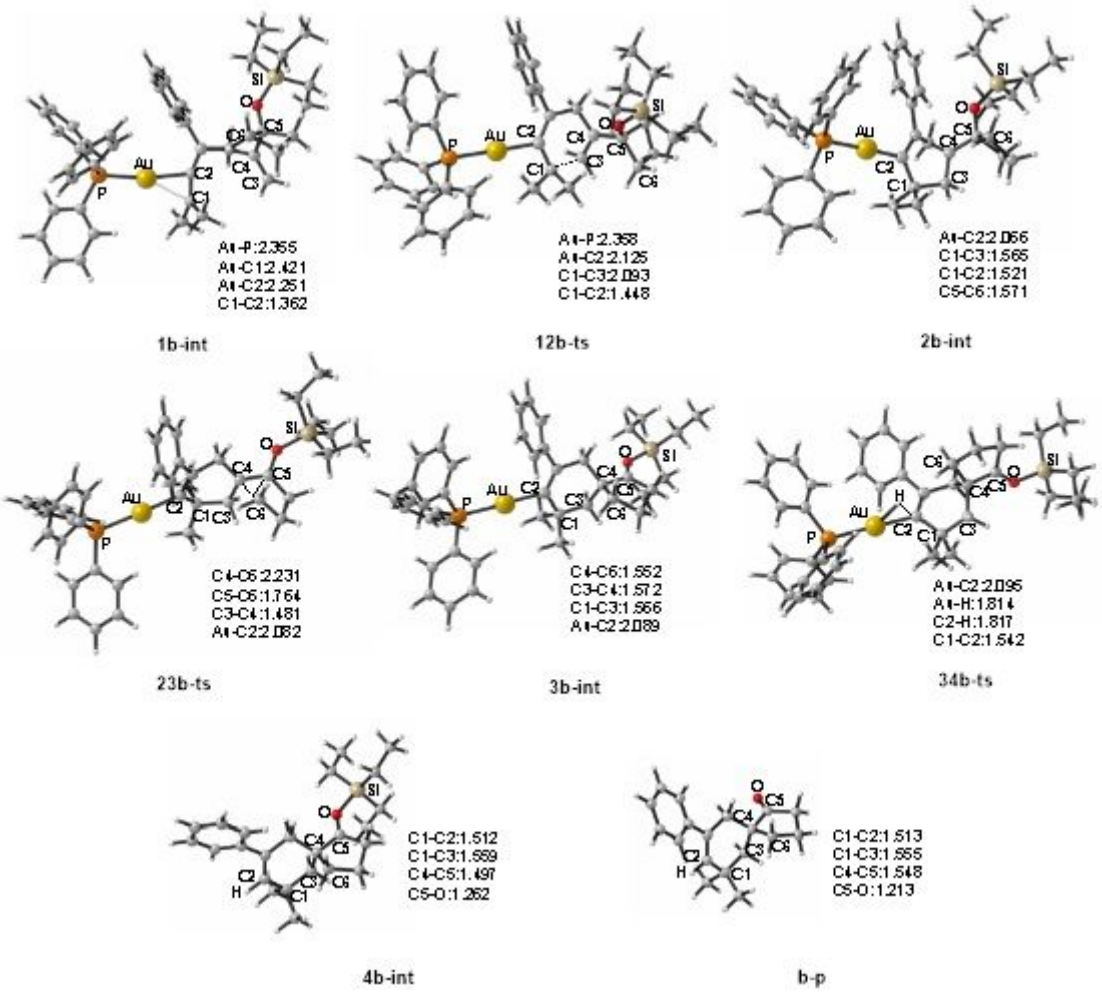

Figure 5

The optimized structures with the key bond lengths in Å for pathway b are shown in Fig.4.

Supplementary Files

This is a list of supplementary files associated with this preprint. Click to download.

- Schemes1and2.pdf